Reac Kinet Mech Cat (2017) 121:185–208
DOI 10.1007/s11144-017-1167-1

Catalytic activity of hydrotalcite-derived catalysts in the dry reforming of methane: on the effect of Ce promotion and feed gas composition

Radosław Dębek[1,2] · Monika Motak[1] · Maria Elena Galvez[2] · Patrick Da Costa[2] · Teresa Grzybek[1]

Received: 30 November 2016 / Accepted: 21 February 2017 / Published online: 15 March 2017

Abstract Ni/Al and Ni/Mg/Al hydrotalcite-derived materials containing various Ni loadings were synthesized and subsequently promoted with Ce-species via adsorption from $[Ce(EDTA)]^-$ complexes. The obtained materials were characterized by elemental analysis (ICP-MS), XRD, H_2-TPR, CO_2-TPD, TG and low temperature N_2 sorption experiments. The amount of the introduced Ce was dependent on the nickel and magnesia content in catalysts precursors, and it influenced materials properties (i.e. basicity, reducibility of Ni species) in various ways and the catalytic performance in the dry reforming of methane (DRM). The promoted catalysts showed improved performance with CH_4 and CO_2 conversions at 550 °C in the range of 35–55 and 35–45%, respectively. The extent of the improvement was dependent on the nickel content and the presence of magnesia. In general, Ce promotion increased materials stability by changing of the type of carbonaceous deposits. Ce modification hindered the transformation of amorphous carbonaceous deposits to graphitic carbon. The former may be easier oxidized and contribute to syngas production. Two selected catalysts were additionally tested in DRM at elevated temperatures (650 and 750 °C) and over various feed gas compositions.

Keywords Hydrotalcite · Nickel · Cerium · CO_2 · Dry reforming

✉ Radosław Dębek
debek@agh.edu.pl; raddebek@gmail.com

[1] Department of Fuels Technology, Faculty of Energy and Fuels, AGH University of Science and Technology, al. A. Mickiewicza 30, 30-059 Kraków, Poland

[2] Sorbonne Universites, UPMC, Univ. Paris 6, CNRS, UMR 7190, Institut Jean Le Rond d'Alembert, 2 Place de la Gare de Ceinture, 78210 Saint-Cyr-L'Ecole, France

Introduction

Despite the trend to limit emissions of carbon dioxide to the environment ongoing for many years, the amount of CO_2 emitted from human activities had increased from 35 billion tons in 2008 [1] to 35.9 billion tons in 2014 [2]. This shows that the reduction of CO_2 emission is still an unsolved problem. The main reason for that is the high consumption of fossil fuels, which is related to the increase in world population as well as the growing consumption [3].

At the beginning of the twenty-first century, great hopes are placed in technologies related to carbon dioxide capture and storage (CCS). However, numerous studies have shown that these methods have major economic and environmental constraints, such as e.g. selecting the appropriate formation for injection. In addition, there is a lack of social acceptance for compressed CO_2 transport and its geological storage. The proposed new technologies are related to the capture and utilization of CO_2 (CCU methods).

Technologies using CO_2 as a substrate are intensively studied now (the production of liquid fuels, DRM, methanation, production of ethanol etc.) [4–7]. Currently, the use of captured CO_2 in industry is estimated to be ca. 5%. However, it is believed that the commercialization of new chemical processes can increase the utilization of the captured CO_2 which could increase up to 10% [8].

Particularly interesting CCU abatement technologies are those that can also be used in the processes of storing energy in chemical products, such as the methanation of CO_2 or the dry reforming of methane. The latter has attracted much attention as it allows the production of synthesis gas with the ratio of CO to H_2 equal to 1, which is required for further chemical processing to fuels e.g. via the Fischer–Tropsch synthesis [9, 10]. The main problem of DRM is, however, the lack of an appropriate catalyst, which is active in this process and simultaneously resistant to carbon deposition [11].

Recently, a lot of attention has been paid to the study of to hydrotalcite-derived materials as possible catalysts for DRM [12–18]. To improve the stability of the Ni-based catalysts, various promoters were proposed. Daza et al. studied the promotion of Ni/Mg/Al hydrotalcite-derived materials with ceria [19–23] and showed that the final effect of Ce was influenced by the method of its introduction [21], loading (the optimal value was established to be ca. 3 wt% [19, 20, 23]), as well as hydrotalcite preparation method [22]. The Ce-promotion improved both the activity and stability of the studied materials. The beneficial effect on the stability may be ascribed to the presence of CeO_2, which reacts with carbon deposited to produce Ce_2O_3 and CO_2 [20]. Other additions studied as promoters to hydrotalcite-derived catalytic systems containing Ni in DRM included lanthanum [24–26], cobalt [27–29], rhodium [30], ruthenium [27] and zirconium [31].

In the present study, various cerium promoted Ni/Al and Ni/Mg/Al hydrotalcite-derived materials were studied. The catalytic activity of the unpromoted materials was presented in our previous work [32]. The goal of this study was to establish how ceria promotion influences catalytic activity of Ni/Al and Ni/Mg/Al hydrotalcite-derived catalysts in DRM. The properties of the prepared materials were mainly

affected by the nickel content and the Ni/Mg molar ratio. However, as shown in previous work, Ce promotion turned out to determine the stability of materials via changing the activity and selectivity of the DRM process. Moreover, for the selected catalysts, which were considered a good representation of Ni/Al and Ni/Mg/Al hydrotalcite-derived materials, the effect of reaction conditions such as temperature and feed gas composition was also examined.

Experimental

Catalyst preparation

The catalysts precursor synthesis was reported elsewhere [32]. In short, five various Ni/Al and Ni/Mg/Al hydrotalcite-like materials were prepared with the value of molar ratio of divalent to trivalent cations in brucite layers fixed at 3. The samples were prepared by the co-precipitation method at constant pH. The nickel content was changed within the samples by the substitution of 5, 25, 50, 75 and 100% of Mg^{2+} by Ni^{2+} cations in the brucite-like layers in comparison to naturally occurring hydrotalcite mineral with chemical formula of $Mg_6Al_2(OH)_{16}CO_3{\cdot}4H_2O$. In this work, the obtained hydrotalcite materials were promoted with Ce species via adsorption from the aqueous solution of $[Ce(EDTA)]^-$ complexes. In order to do that, hydrotalcite powders were mixed with the 3 wt% solution of $[Ce(EDTA)]^-$ complexes for 24 h at room temperature. The exact procedure is described elsewhere [31, 33]. The Ce-promoted catalysts were calcined in the stream of air at 550 °C for 4 h. The designation of the catalysts includes the percentage of Mg exchanged for Ni, as well as the presence (or absence) of cerium promoter, e.g. HTNi25-Ce and HTNi100 refer to hydrotalcite with 25% Mg replaced by Ni promoted with additionally cerium present in the sample, and hydrotalcite, where all Mg was replaced by Ni without Ce promotion. The designation of the prepared catalysts and their nominal composition is presented in Table 1.

Physicochemical characterization

The structure of cerium promoted catalysts was determined in this work and compared to unpromoted hydrotalcite precursors described previously in [32]. The catalysts obtained upon their calcination and after catalytic tests were examined by means of XRD experiments. The diffractograms were recorded in the 2θ range from 8° to 90° on Empyrean diffractometer from PANalytical, using Cu K_α radiation ($\lambda = 0.154059$ nm). The catalysts' elemental composition was determined by inductively coupled plasma mass spectrometry. The ICP-MS measurements were carried out by "SCU du CERN". The reducibility of the catalysts was evaluated by temperature programmed reduction of H_2 (H_2-TPR) on a BELCAT-M apparatus from BEL Japan equipped with a thermal conductivity detector. 50 mg of a sample was degassed at 100 °C for 2 h. The sample was subsequently reduced in 5% (vol/vol) H_2/Ar from 100 to 900 °C at 7.5 °C/min heating rate. The BELCAT-M apparatus from BEL Japan was also used to evaluate the basicity of the materials by

Table 1 The designation of prepared materials and details of the preparation procedure

Sample name	Cations in brucite layers	Ni/Mg molar ratio	M^{2+}/M^{3+} molar ratio	Absorption of $[Ce(EDTA)]^-$ complexes
HNi5	Ni^{2+}, Mg^{2+}, Al^{3+}	0.05	3	–
HNi5-Ce	Ni^{2+}, Mg^{2+}, Al^{3+}	0.05	3	+
HNi25	Ni^{2+}, Mg^{2+}, Al^{3+}	0.33	3	–
HNi25-Ce	Ni^{2+}, Mg^{2+}, Al^{3+}	0.33	3	+
HNi50	Ni^{2+}, Mg^{2+}, Al^{3+}	1.0	3	–
HNi50-Ce	Ni^{2+}, Mg^{2+}, Al^{3+}	1.0	3	+
HNi75	Ni^{2+}, Mg^{2+}, Al^{3+}	3.0	3	–
HNi75-Ce	Ni^{2+}, Mg^{2+}, Al^{3+}	3.0	3	+
HNi100	Ni^{2+}, Al^{3+}	–	3	–
HNi100-Ce	Ni^{2+}, Al^{3+}	–	3	+

Values for unpromoted catalysts were adapted from [32]

the temperature programmed desorption of CO_2 (CO_2-TPD). The measurements were performed for the reduced samples. The materials (60 mg) were first degassed for 2 h at 500 °C and then cooled to 80 °C. A mixture of 10% (vol/vol) CO_2/He was then introduced for 1 h in order to adsorb CO_2. A flow of helium was subsequently fed for 15 min to desorb weakly physically adsorbed CO_2. The samples were further heated up to 800 °C under He flow at the heating rate of 10 °C/min, while the evolution of CO_2 was measured with the aid of a TC detector. The textural properties of the catalysts were determined from low temperature N_2 sorption isotherms obtained during experiments carried out on Belsorp Mini II apparatus from BEL Japan. Prior to each measurement, mixed oxide powders were degassed under vacuum for 3 h at 110 °C. Carbon formation during the DRM reaction was quantified using thermogravimetric analysis under air atmosphere. The experiments were carried out with a SDT Q600 apparatus (TA Instruments), under an air flow of 100 cm^3/min with heating from ambient temperature to 900 °C at a rate of 10 °C/min.

Dry reforming of methane

The DRM catalytic tests for cerium promoted catalysts were carried out in the fixed-bed U-shaped quartz reactor heated inside a resistance oven. The tested catalysts were present in the powder form with the grain size between 0.09–0.16 mm. In a typical experiment 150–200 mg of catalyst was tested, depending on its bulk density. The temperature of the catalyst bed was controlled with the aid of a K-type thermocouple. The total flow of feed gases was controlled by a series of mass-low controllers (BROOKS) and was equal to 100 cm^3/min, corresponding to the GHSV of 20,000 h^{-1}. The products of the reaction were analyzed by an on-line Varian GC490 micro chromatograph equipped with a TCD detector. Prior to each catalytic test, a catalyst was reduced in the stream of 5% H_2 in Ar for 1 h at 900 °C. The

catalyst bed was then flushed with Ar and cooled down to the desired temperature (550, 650 or 750 °C) and feed gases were introduced. Most of the catalytic tests were carried out with the feed gas composition of $CH_4/CO_2/Ar = 1/1/8$. For a selection of catalysts, additional DRM runs were performed with the excess of CH_4 ($CH_4/CO_2/Ar = 1.5/1/7.5$), the excess of CO_2 ($CH_4/CO_2/Ar = 1/1.5/7.5$), the increased concentrations of both CH_4 and CO_2 in the feed ($CH_4/CO_2/Ar = 1.5/1.5/7$) and finally for direct methane decomposition ($CH_4/CO_2/Ar = 2/0/8$). The results of DRM tests carried out for the unpromoted catalysts under the same conditions were discussed in the previous paper [32].

Results and discussion

Physicochemical features of Ce-doped hydrotalcite derived Mg(Ni, Al)O materials

Table 2 shows the composition of various Ce promoted hydrotalcite-derived catalysts, as determined by ICP-MS analysis. A Ni content between 4–60 wt% was determined for the studied catalysts. Ni/Mg and M^{2+}/M^{3+} molar ratios were in each case close to the nominal values assumed at the co-precipitation stage as discussed previously [32]. The Ce content in all samples decreased with the increasing content of Ni. In general, the adsorption of $[Ce(EDTA)^-]$ complexes resulted in the introduction 1.4 to ca. 4 wt% of cerium species.

The XRD patterns acquired for the fresh Ce-promoted hydrotalcites, as well as the calcined HT-derived catalysts are compared in Fig. 1a and 1b with the unpromoted materials. Before calcination (Fig. 1a), all promoted and unpromoted materials showed a typical layered structure of hydrotalcite [34–36]. The absence of any other additional crystalline phase in the diffractograms of Ni-HTs or Ni–Ce-HTs indicates first the successful incorporation of nickel cations into the brucite-like layers. Second, it confirms that the adsorption of $[Ce(EDTA)]^-$ species (cp. Table 2) led to the good distribution of cerium on the catalyst surface, as confirmed by the absence of any cerium-containing phase in XRD. The unit cell parameters calculated for obtained hydrotalcites (Table 3) showed that there was no significant

Table 2 Results of elemental analysis for ceria promoted catalysts

Sample	Ni (wt%)	Mg (wt%)	Al (wt%)	Ce (wt%)	Ni^{2+}/Mg^{2+a}	M^{2+}/M^{3+a}
HTNi5-Ce	4.3	24.0	11.7	4.1	0.04 (0.05)	2.96 (3.0)
HTNi25-Ce	17.9	21.5	10.8	3.7	0.34 (0.33)	2.96 (3.0)
HTNi50-Ce	32.9	13.3	10.1	2.6	1.03 (1.0)	2.96 (3.0)
HTNi75-Ce	48.6	6.4	10.2	1.9	3.08 (3.0)	2.89 (3.0)
HTNi100-Ce	59.0	–	8.9	1.4	–	3.05 (3.0)

[a] Molar ratio, in parenthesis nominal values are given

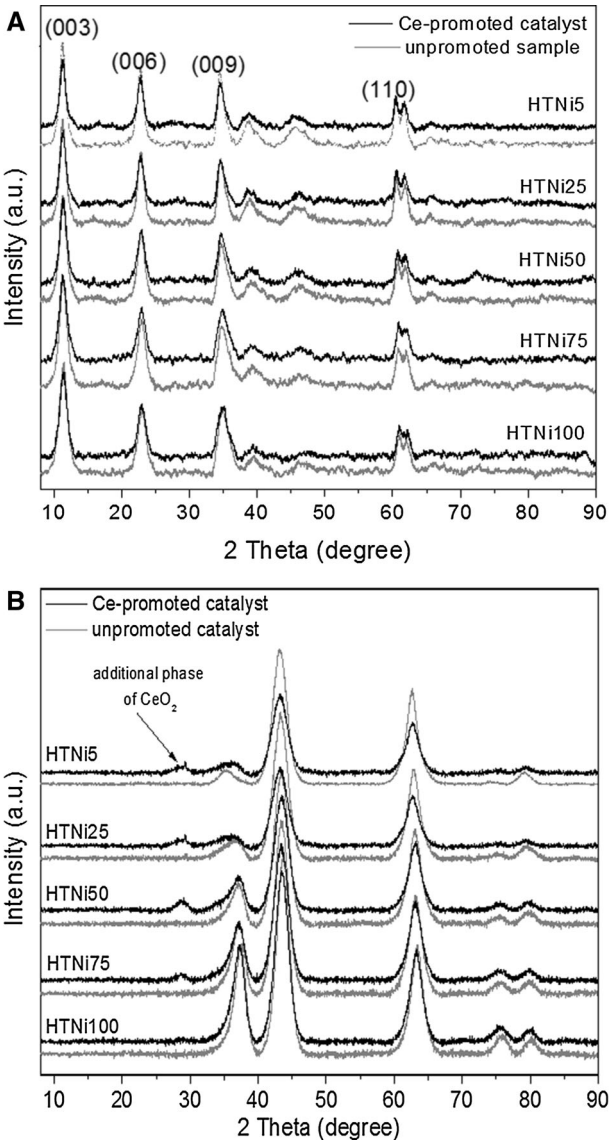

Fig. 1 XRD diffractograms for: **a** fresh hydrotalcites and **b** calcined materials

increase in the basal spacing between hydrotalcite layers (values of parameters c and c'), indicating that adsorption of $[Ce(EDTA)]^-$ species did not result in ion exchange, and cerium species were most probably deposited on the external surfaces of crystallites. All values of c and c' were within the range typical for CO_3^{2-} (7.65 Å) and NO_3^- (8.79 Å) [34].

The XRD diffractograms corresponding to the calcined catalysts (Fig. 1b), show two main reflections at 43° and 64° 2θ, ascribed to Mg(Ni,Al)O mixed oxides with

Table 3 Unit cell parameters and type of anions present in the interlayer spaces of hydrotalcites promoted with ceria (uncalcined samples) Adapted from [32]

Sample	Unit cell parameter a^a (Å)	Unit cell parameter c^a (Å)	$c' = c/3^a$ (Å)	Anions between brucite-layers
HTNi5-Ce	3.06 (3.06)	23.43 (23.52)	7.81 (7.84)	CO_3^{2-} and NO_3^-
HTNi25-Ce	3.06 (3.06)	23.37 (23.43)	7.79 (7.81)	CO_3^{2-} and NO_3^-
HTNi50-Ce	3.06 (3.06)	23.28 (23.40)	7.76 (7.80)	CO_3^{2-} and NO_3^-
HTNi75-Ce	3.06 (3.06)	23.31 (23.31)	7.77 (7.77)	CO_3^{2-} and NO_3^-
HTNi100-Ce	3.06 (3.06)	23.22 (23.25)	7.74 (7.75)	CO_3^{2-} and NO_3^-

[a] In parenthesis are given values for unpromoted samples

periclase structure formed upon thermal decomposition of hydrotalcite materials [37, 38]. Additionally, for all Ce-promoted catalysts low intensity reflections observed at ca. 28° and 37° 2θ were registered, pointing to the presence of cubic fluorite structure of CeO_2 (ICOD 00-023-1048). The intensity of this reflection increased with the decreasing Ni loading, suggesting that nickel content in brucite layers influenced the amount of cerium species that could be introduced into catalytic system via adsorption procedure.

The values of textural parameters i.e. specific surface area, S_{BET}, total pore volume, V_{tot}, and mean pore diameter, d_p, calculated from the N_2 adsorption isotherms for different HT-derived catalysts promoted with Ce are compared with the unpromoted catalysts in Table 4. All values of textural parameters are typical for mesoporous hydrotalcite-derived mixed oxides [34, 39, 40]. The Ce doping did not significantly change the textural properties, since for Ce-promoted materials were at a similar level as for the parental ones, with the exception of the sample loaded with the lowest amount of Ni. As discussed before, the amount of introduced Ce species via adsorption was dependent on Ni/Mg molar ratio and was increasing with the decrease in Ni/Mg (see Table 2). Thus, one could expect that with the increasing amount of ceria species on the catalyst surface a partial blockage of pores may appear, leading to the decrease of S_{BET} and V_{tot}. In the case of the two catalysts

Table 4 Textural properties of Ce promoted calcined materials and the total basicity for the reduced samples Adapted from [32]

Sample	Texture[a]			Total basicity[a] (μmol/g)
	S_{BET} (m^2/g)	V_{tot} (cm^3/g)	d_p (nm)	
HTNi5-Ce	113 (167)	0.54 (0.74)	19 (18)	45 (60)
HTNi25-Ce	102 (114)	0.33 (0.41)	13 (14)	91 (104)
HTNi50-Ce	113 (126)	0.31 (0.35)	11 (11)	70 (83)
HTNi75-Ce	131 (127)	0.28 (0.29)	8 (9)	43 (51)
HTNi100-Ce	123 (122)	0.54 (0.61)	18 (20)	30 (37)

[a] In the parenthesis values for unpromoted catalysts are given

loaded with the highest nickel content (samples HTNi75-Ce and HTNi100-Ce), a small increase in the values of S_{BET} and V_{tot} was observed, suggesting that for these two samples the ceria deposition was a source of additional porosity. This proves that the effect of ceria promotion is strongly affected by the Ni/Mg molar ratio.

Total basicity of the reduced samples was measured with the aid of CO_2-TPD experiments. The results of the analysis are presented in Table 4. The ceria addition resulted in the decrease of total basicity for all catalysts. A similar effect was observed for HTNi25-Ce catalyst, as reported in our previous work [41]. It was observed, however, that the decrease of total basicity was compensated by the increase in the concentration of intermediate and strong basic sites, which are associated with Lewis acid–base metal–oxygen pairs and low coordinated oxygen anions (strong basic Lewis sites), respectively [40, 42, 43].

The H_2-TPR profiles obtained for the catalysts doped with Ce are compared to the unpromoted materials in Fig. 2. All catalysts showed one asymmetric reduction peak, which was centered between 400–800 °C for the samples with high nickel loading and at 600–900 °C for the samples with Ni loadings lower than 20 wt%. The Ni/Mg molar ratio had an influence on the shape and maximum reduction temperature of the reduction peaks. The shift to higher reduction temperatures occurred with the decreasing nickel loading. This may be explained by the formation of smaller nickel crystallites with stronger interactions between the active phase and the support, as reported in [32].

The position of maximum temperature of reduction (T_{max}) was dependent on the presence of the Ce-promoter as well. The shift was dependent on Ni content in the sample. T_{max} was shifted to higher temperature for the ceria promoted sample HTNi100-Ce with the high nickel loading, indicating the decrease in catalyst reducibility after the small ceria addition. For the samples HTNi50-Ce and HTNi75-Ce, ceria addition practically did not influence reducibility. In contrast, the opposite effect was observed for the samples with Ni loading lower than 20 wt%, i.e.

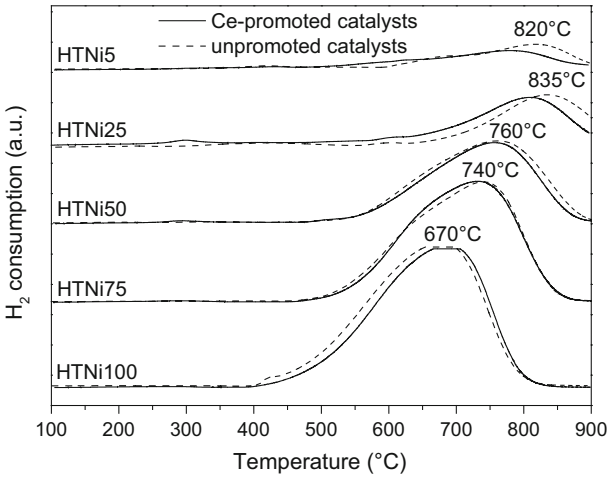

Fig. 2 H_2-TPR profiles registered for Ce-promoted catalysts and their parental materials

HTNi25-Ce and HTNi5-Ce. T_{max} was shifted from 810 to 835 °C and from 780 to 820 °C for HTNi25-Ce and HTNi5-Ce, respectively when compared to the unpromoted samples. These results are in good agreement with those reported in the literature [19–21]. The different trend for samples with or without Mg in its structure (HTNi100-Ce as compared to other catalysts) also suggests that the reducibility is an overlapping effect originating from the presence of both ceria and magnesium in the catalysts. In the absence of Mg in the HT-derived catalyst (HTNi100-Ce), reducibility increased. The increasing amount of Mg in the catalysts shifted the reduction peak to higher temperatures as compared to HTNi-Ce. However, the effect may have been additionally complicated by the fact that the content of magnesia is dependent on the Ni content.

The Ce-promoted catalysts exhibited additionally reduction peaks of very low intensity centered at ca. 250, 300, 415 and 600 °C. In this temperature region, the reduction process is quite complicated to explain since both processes of the reduction of NiO and ceria may have overlapped. The reduction of pure CeO_2 occurs in three stages: (i) the reduction of surface oxygen or oxygen capping species (250–300 °C) [44], (ii) the reduction of surface lattice oxygen (450–600 °C) [23] and total bulk reduction up to 900 °C [21]. On the other hand, the reduction of Ni species from the framework of Mg(Ni,Al)O mixed oxides to metallic nickel is realized in two steps: (i) the reduction of surface NiO (ca. 420 °C) [45, 46] and (ii) the reduction of NiO strongly interacting with the support (600–800 °C) [18, 47]. As ceria species were introduced via adsorption, they are most probably deposited over Mg(Ni,Al)O mixed oxides phase, and thus the additional reduction peaks may be explained by the reduction of Ce^{4+} to Ce^{3+}.

Low temperature DRM with stoichiometric mixture of substrates

The effect of ceria promotion was first evaluated during isothermal DRM runs at 550 °C. The results of catalytic tests for ceria promoted catalysts are presented in Fig. 3 in comparison with the parental materials. The effect of the addition of cerium species was dependent on the content of nickel in the catalysts and the presence of magnesia. The Ce-promoted sample derived from Ni/Al hydrotalcite-like material (HTNi100-Ce), the sample with the high Ni content (HTNi75-Ce) and their corresponding parental materials exhibited higher conversions of CH_4 than those of CO_2. The conversions of CH_4 higher than those of CO_2 resulted also in the excess of H_2 in the products of the reaction. The effect of ceria promotion for these two Ce-promoted catalysts was dependent on the presence of magnesia. Sample HTNi100-Ce exhibited increased conversion of CH_4 with respect to unpromoted catalyst, suggesting the occurrence of direct methane decomposition. The magnesia containing catalyst (sample HTNi75-Ce) showed a decrease in activity when compared to the unpromoted catalyst. The opposite trend was observed for Ni/Mg/Al hydrotalcite derived materials with Ni contents around 20 wt%. In this case, the ceria promotion resulted in decreased conversions of CH_4 but higher conversions of CO_2 in comparison to the respective unpromoted catalyst. The sample with the lowest content of Ni exhibited decrease in both CH_4 and CO_2 conversions.

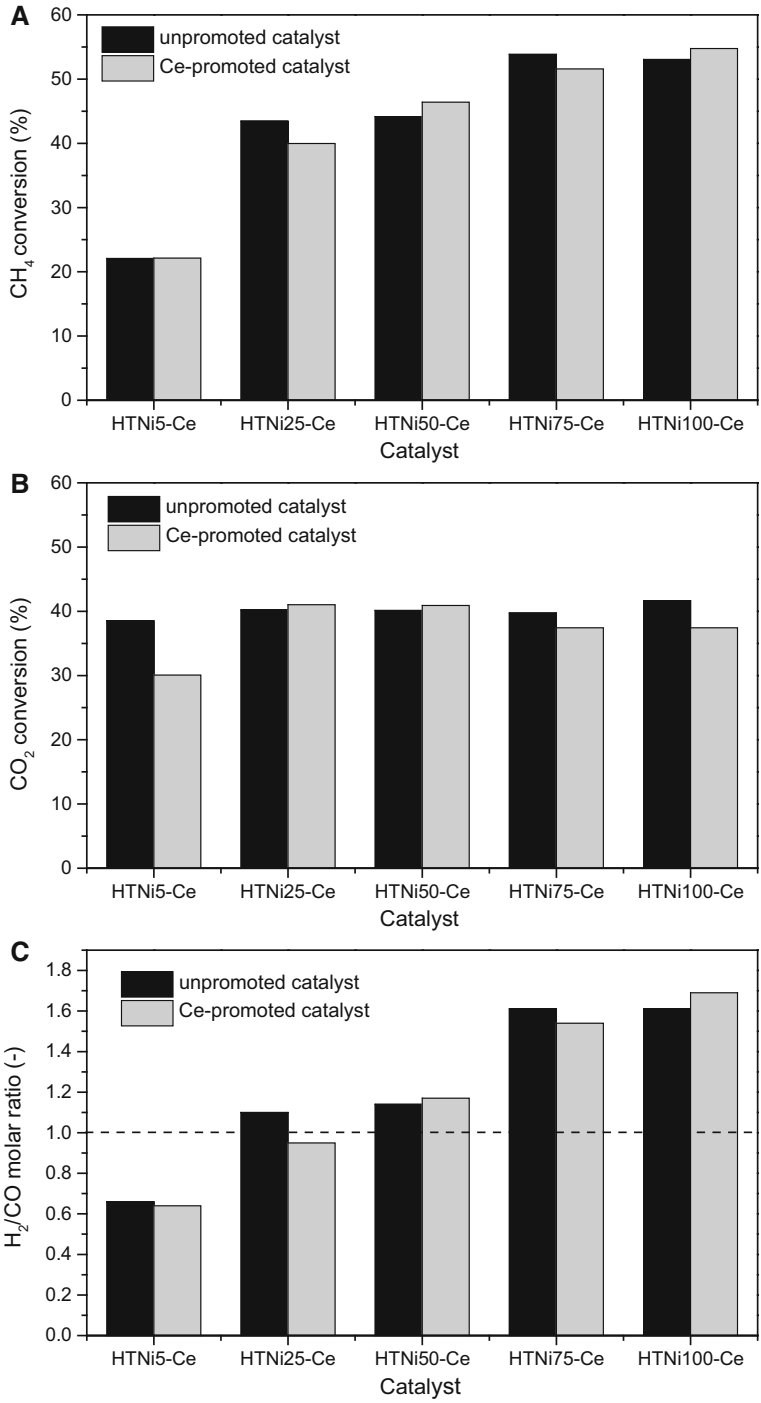
A
unpromoted catalyst
Ce-promoted catalyst
CH4 conversion (%)
0
10
20
30
40
50
60
HTNi5-Ce
HTNi25-Ce
HTNi50-Ce
HTNi75-Ce
HTNi100-Ce
Catalyst
B
unpromoted catalyst
Ce-promoted catalyst
CO2 conversion (%)
0
10
20
30
40
50
60
HTNi5-Ce
HTNi25-Ce
HTNi50-Ce
HTNi75-Ce
HTNi100-Ce
Catalyst
C
unpromoted catalyst
Ce-promoted catalyst
H2/CO molar ratio (-)
0.0
0.2
0.4
0.6
0.8
1.0
1.2
1.4
1.6
1.8
HTNi5-Ce
HTNi25-Ce
HTNi50-Ce
HTNi75-Ce
HTNi100-Ce
Catalyst

◀**Fig. 3** The comparison of catalytic performance in DRM at 550 °C of Ce-promoted and unpromoted catalysts. Average values registered during 5 h catalytic tests: **a** CH_4 conversion, **b** CO_2 conversion and **c** H_2/CO molar ratio; GHSV = 20,000 h^{-1}; $CH_4/CO_2/Ar$ = 1/1/8; total flow 100 cm^3/min

Ce-promotion influenced as well the distribution of the obtained products. The samples with the high and medium content of nickel (above ca. 32 wt%) exhibited the excess of H_2 in the products of the reaction, while the HTNi5-Ce catalyst showed the opposite trend, with the excess of carbon monoxide. As reported in our previous research [32], the Ni loading influenced the occurrence of side reactions, CH_4 decomposition and reverse water gas shift (RWGS). The former proceeds more easily with the increasing content of Ni, while RWGS is more developed over catalysts with low Ni content. Ce-promoted samples exhibited the same trends as the unpromoted catalysts (Fig. 3).

Reported in the literature thermodynamic limitations relevant to the conditions applied in this study for DRM at 550 °C showed that equilibrium conversion of CH_4, CO_2 and H_2/CO molar ratio are respectively equal to ca. 87, 45% and 3.5 [48]. This suggest that at tested temperature direct methane conversion is well developed, leading to high production of H_2 and much higher conversion of CH_4 than CO_2. Considering thermodynamic limitations and the results presented in Fig. 3, it may be seen that the CO_2 conversions were close to thermodynamic limit for all tested samples. This effect was enhanced by the ceria promotion for HTNi25-Ce and HTNi50-Ce catalysts which exhibited higher conversions of CO_2 than the unpromoted materials. Both the CH_4 conversions and the H_2/CO molar ratio were much lower than the equilibrium values, indicating that the applied catalysts changed the selectivity of the process and inhibited direct CH_4 decomposition reaction. Moreover, this effect is strongly dependent on the presence of magnesia and Ni/Mg molar ratio. The Ce promotion enhanced this effect for magnesia containing samples.

For all catalysts, both promoted with Ce and unpromoted, the decrease in CO_2 conversion was observed during the first 100 min of reaction (results not shown; for HTNi100-Ce and HTNi25-Ce these results are presented in Figs. 8 and 9), which may account, to a certain extent, for catalyst deactivation and loss of selectivity towards DRM. However, the positive effect of ceria promotion on the stability of the catalysts was observed, as CO_2 conversions for Ce-containing samples stabilized within a shorter period of time than in the case of unpromoted catalysts. Moreover, CO_2 conversions reached higher values for HTNi25-Ce and HTNi50-Ce than for the respective unpromoted samples. According to Daza et al. [23], the promoting effect of ceria is due to the Mg and Ce synergetic effect on CO_2 adsorption capacity. As confirmed by CO_2-TPD experiments, the HTNi100-Ce and HTNi75-Ce samples exhibited the lowest values of total basicity (Table 4), which was caused, among others, by the absence of magnesia in the catalyst structure in the former sample and the presence of only small amount of MgO in the latter. Therefore, the different effect of ceria promotion on the prepared catalysts may be explained by the lack of synergetic effect between Ce and Mg, which enhances the basicity of the material.

The XRD diffractograms obtained for the spent catalysts after 5 h DRM tests are presented in Fig. 4. All samples, with the exception of HTNi5-Ce, exhibited the

presence of the reflections characteristic for graphitic carbon (2θ equal to ca. 26°), which was obviously formed during DRM tests. The intensity of this reflection, when compared to the parental materials, was dependent on the Ni content and the presence of magnesia. Ce-promoted Ni/Al derived sample exhibited higher intensity of the reflection originating form graphitic carbon than the unpromoted sample, while all Mg-containing materials showed the opposite trend. This clearly illustrates the positive effect of the co-existence of ceria and magnesia on the possible decrease in the formation of graphitic carbon on Ni/Mg/Al derived hydrotalcites.

In order to determine the amount of the formed carbon deposits, TG experiments were performed for two selected catalysts (HTNi100-Ce and HTNi25-Ce) and the respective samples without cerium (Fig. 5). The mass loss for Ce-containing samples was higher than for the corresponding samples without Ce. The comparison with XRD patterns for the appropriate samples indicates that not only graphitic carbon was deposited on the surface. Apparently, other carbon forms are also present. This is additionally proven by DTG curves. The appropriate maxima are shifted for ceria promoted catalysts to lower temperatures—from 610 to 590 °C for HTNi100 and HTNi100-Ce, respectively, and from 575 to 555 °C for HTNi25 and HTNi25-Ce. This indicates that the Ce addition promoted side reactions other than CH_4 decomposition, leading to the formation of different carbonaceous deposits with respect to the unpromoted catalysts. The possible reaction leading to carbon deposits could be reduction of CO_2 with H_2 to C and water. This could explain the increase in CO_2 conversion for HTNi25-Ce catalyst compared to the catalyst HTNi25 (Fig. 3b). On the other hand, as the decrease in CO_2 conversion and higher

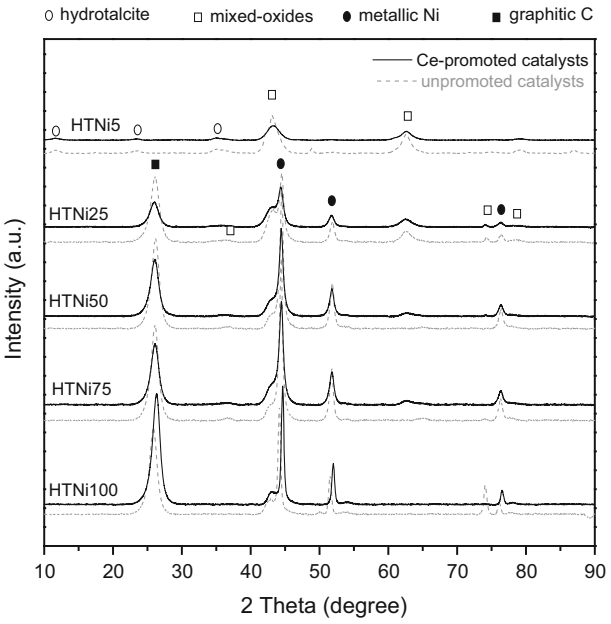

Fig. 4 XRD diffractograms registered for the catalysts after 5 h DRM runs at 550 °C

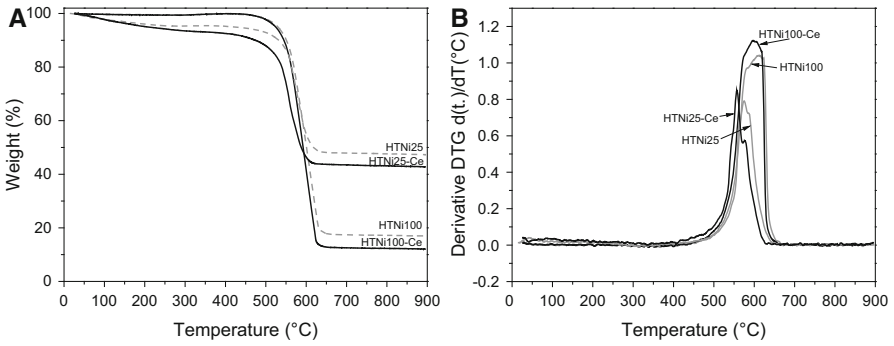

Fig. 5 Results of TG experiments performed for Ce-promoted catalysts and their parental materials after DRM tests carried out at 550 °C

deposition of coke was observed for HTNi100-Ce sample, when compared to its parental, the carbon deposit for this catalyst might have been formed, to a higher extent, by disproportionation of CO.

It is worth mentioning that the addition of ceria for both HTNi25 and HTNi100 led to a shift of DTG peaks to lower temperatures, indicating that ceria promoted the oxidation of carbon deposits. The DTG peaks observed for all catalysts were centered at temperatures between 550–650 °C and was formed via the overlapping of at least two exothermic peaks, suggesting the formation of at least two type of carbon deposits, most probably amorphous and graphitic carbon [17, 49, 50]. The formation of the latter during DRM reaction at 550 °C was confirmed by XRD.

On the influence of reaction temperature

Catalysts HTNi100-Ce and HTNi25-Ce were chosen for additional catalytic tests at elevated temperatures (650 and 750 °C). The obtained results were compared to HTNi100 and HTNi25 [32]. The results of the tests at 550 °C and the materials characterization suggest that they are a good representation of Ni/Al and Ni/Mg/Al hydrotalcite-derived materials and, therefore, they were chosen for these additional DRM runs. The comparison of the catalysts performance, given as average CH_4, CO_2 conversions and H_2/CO molar ratio as a function of temperature, is presented in Fig. 6 for Ce-promoted and unpromoted catalysts. The effect of ceria addition was the same for 650 and 750 °C. It resulted in decreased conversions of CH_4 and increased conversions of CO_2 with respect to unpromoted catalysts. Moreover, at 750 °C, the product distribution, i.e. values of H_2/CO molar ratio, was the same for Ce-promoted and unpromoted catalysts. The effect of ceria promotion was more evident for sample HTNi25-Ce, which was loaded with higher ceria content, than for the HTNi100-Ce sample. The H_2/CO molar ratio decreased in comparison to the parental material and the differences between unpromoted and promoted catalysts were decreasing with the increase in temperature. Over the tested temperature range, CH_4 conversions were higher than CO_2 conversions for Ni/Al derived catalyst. Similar results were obtained for HTNi25 sample at 550 and 650 °C. Only for

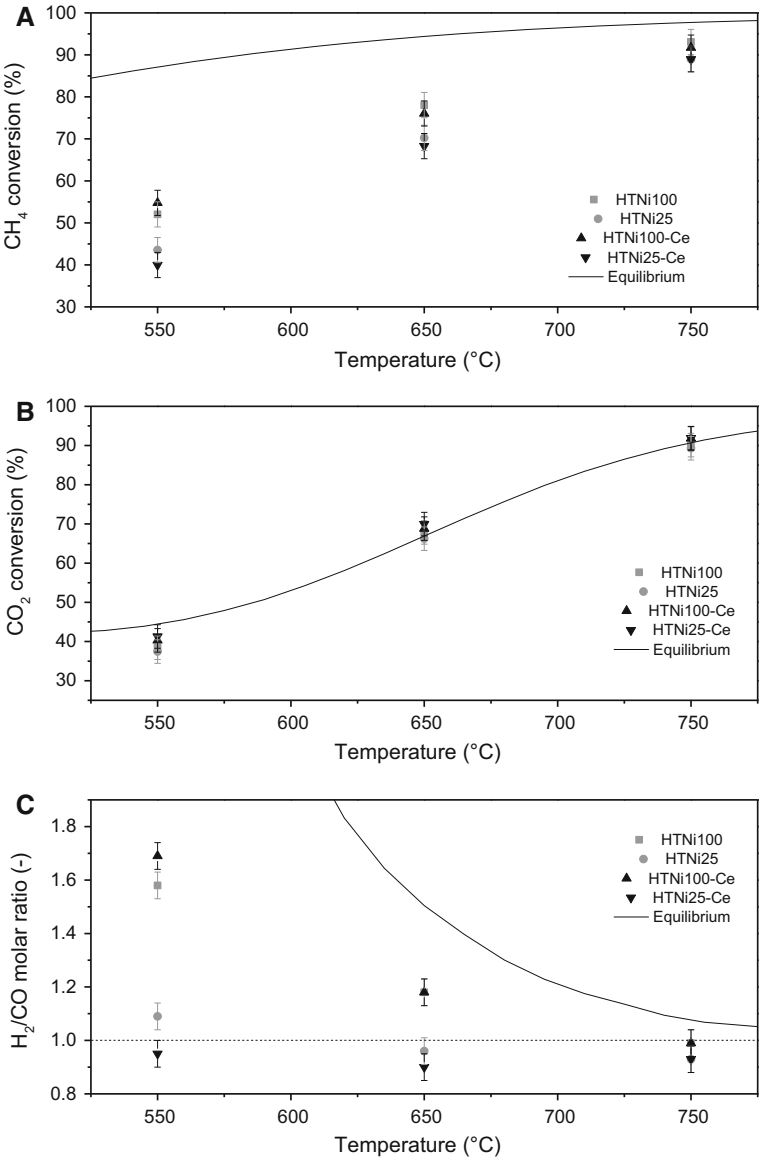

Fig. 6 Catalytic tests over Ce-promoted catalysts at 550, 650 and 750 °C in comparison to unpromoted samples. The average values of CH_4 (**a**) and CO_2 conversions (**b**) and H_2/CO molar ratio (**c**) registered during isothermal 5 h TOS DRM runs; GHSV = 20,000 h^{-1}; $CH_4/CO_2/Ar$ = 1/1/8; total flow 100 cm^3/min

HTNi25-Ce catalyst, the registered values of CO_2 conversion were higher than those of CH_4 at all three tested temperatures, suggesting that Ce addition to HTNi25 resulted in the promotion of RWGS reaction, influencing the distribution of the obtained products in this way.

The XRD diffractograms registered for the samples after 5 h of tests at 650 and 750 °C are compared to those after the test at 550 °C in Fig. 7. All catalysts exhibited a reflection at 2θ equal to 26° characteristic of graphitic carbon. Its intensity decreased with the increase in temperature, pointing to the decrease in carbon formation. For the HNi25 and HNi25-Ce catalysts, no graphitic carbon was registered after the tests at 750 °C. Moreover, comparing the respective Ce-promoted catalyst and HTNi25 sample, the lower intensity of graphitic reflection may be observed for the former, indicating that the ceria addition resulted either in the inhibition of the formation of graphitic carbon or faster removal in situ due to a side reaction (reverse Boudouard reaction). Graphitic carbon is considered to be inactive in DRM and hard to oxidize, while amorphous carbon deposits may be oxidized upon DRM contributing to syngas production in this way [49, 50]. Therefore, although Ce promotion resulted in the formation of higher amounts of coke deposits, it also influenced the type of carbonaceous species formed on the catalyst surface, and, as a final result, had a positive effect on the catalyst performance. Interestingly, the HTNi25-Ce catalyst after tests at 750 °C showed the presence of reflections characteristic for the hydrotalcite structure, pointing to the occurrence of 'memory effect', which suggests that RWGS reaction was well developed over the catalyst tested at 750 °C and confirmed previously drawn conclusions.

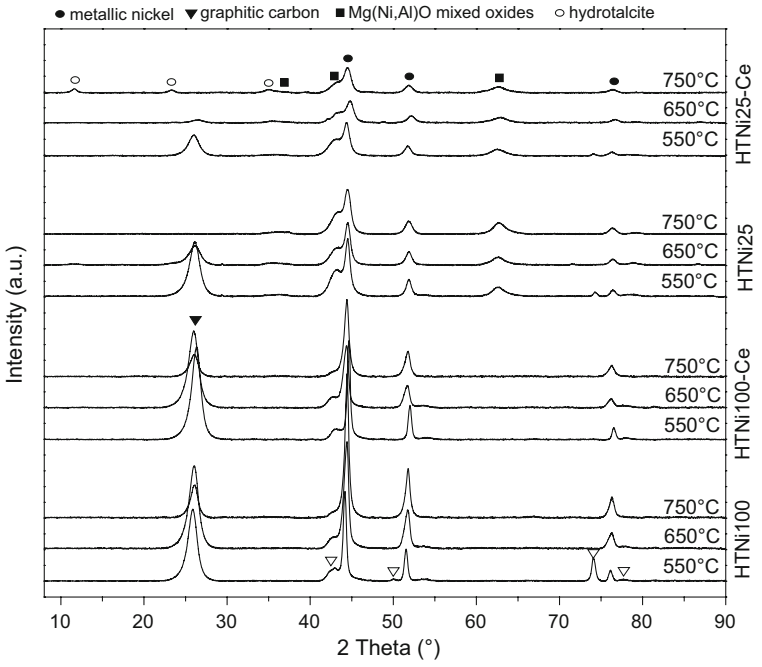

Fig. 7 The XRD patterns recorded for the spent catalysts after DRM runs at 550, 650 and 750 °C for Ce-promoted catalysts and their parental materials

Most DRM catalysts described in the literature suffer from deactivation due to sintering at the high temperature used for the reaction, as well as from carbon deposits [51]. In order to examine the possible sintering of active material, the nickel particle sizes of the reduced and spent catalysts, estimated using the Scherrer equation, are compared in Table 5 for the studied hydrotalcite-derived materials with or without the addition of cerium. It is obvious from Table 5 that the addition of cerium does not affect the tendency to sintering of Ni for the HTNi100 negatively, as proven by very similar Ni particle size after the tests at 550 °C. When HTNi25 and HTNi25-Ce are compared, the positive effect of the addition of Ce may be seen, reflected by the unchanging size of Ni crystallites for the latter after 550 °C test as compared to the reduced sample. For HTNi100, as well as for HTNi100-Ce spent catalyst after tests carried out at 650 and 750 °C Ni crystallites are even smaller than for the appropriate reduced sample, which might explain the observed reduction in the formation of graphitic carbon with the increase in reaction temperature (see Fig. 7). For HTNi25 and HTN25-Ce, this effect is rather small, though the tendency is similar. This suggests some redispersion of Ni crystallites and is rather difficult to explain at the current stage. The effect will need some more experimental data and will be addressed in more detail in our future work.

On the effect of the feed gas composition

The Ce-promoted and the corresponding unpromoted catalysts were also tested in DRM at 550 °C with different compositions of feed gas, i.e. the excess of CH_4, the excess of CO_2 or higher concentrations of CH_4 and CO_2 in comparison to the tests carried out for CH_4/CO_2/Ar ratio of 1/1/8. Table 6 summarizes the results obtained during DRM runs with various feed gas compositions. Some general conclusions may be drawn by analyzing Table 6. The change in the dilution of the reagents (excess of CH_4, excess of CO_2 and excess of both CH_4 and CO_2) resulted in decrease of catalytic activity towards CH_4 and CO_2 with the exception of sample HTNi100-Ce tested over the excess of CH_4 (Table 6; Fig. 8). Moreover, for all samples, excess of CH_4 resulted in increased values of H_2/CO. On the other hand, the excess of CO_2 and the decrease in the dilution of reagents resulted in the decrease of H_2/CO. These results are in agreement with thermodynamic predictions reported in literature [48].

Table 5 The Ni particle size estimated for the reduced and spent samples after DRM runs at 550, 650 and 750 °C

Sample	Ni particle size for reduced catalysts (nm)	Ni particle size for catalysts after DRM tests (nm)		
		At 550 °C	At 650 °C	At 750 °C
HTNi100	20	18	14	15
HTNi100-Ce	19	19	11	12
HTNi25	6	11	9	8
HTNi25-Ce	8	8	7	7

Table 6 The average results of CH_4, CO_2 conversions and H_2/CO molar ratio obtained during 5 h DRM runs over various feed gas compositions for Ce-promoted and corresponding unpromoted catalysts; total flow 100 cm^3/min; GHSV = 20,000 h^{-1}; temperature 550 °C

Sample	Composition of the feed gas $CH_4/CO_2/Ar$	Average CH_4 conversion[a] (%)	Average CO_2 conversion[a] (%)	Average H_2/CO molar ratio[a]
HTNi25	1/1/8	43.4	40.2	1.1
	1.5/1/7.5	37.4 ↓	39.8 ↓	1.5 ↑
	1/1.5/7.5	39.0 ↓	30.4 ↓	0.80 ↓
	1.5/1.5/7	31.9 ↓	34.8 ↓	0.88 ↓
	2/0/8	27.5	–	–
HTNi25-Ce	1/1/8	40.0	41.0	0.95
	1.5/1/7.5	28.1 ↓	39.6 ↓	0.97 ↑
	1/1.5/7.5	29.2 ↓	26.7 ↓	0.65 ↓
	1.5/1.5/7	29.5 ↓	33.4 ↓	0.72 ↓
	2/0/8	22.1	–	–
HTNi100	1/1/8	53.0	41.7	1.6
	1.5/1/7.5	45,6 ↓	39.9 ↓	2.2 ↑
	1/1.5/7.5	52.8 ↓	30.7 ↓	1.3 ↓
	1.5/1.5/7	41.9 ↓	30.1 ↓	1.6 ↓
	2/0/8	31.1	–	–
HTNi100-Ce	1/1/8	54.8	37.4	1.7
	1.5/1/7.5	44.3 ↓	40.0 ↑	2.0 ↑
	1/1.5/7.5	42.2 ↓	26.4 ↓	1.1 ↓
	1.5/1.5/7	40.4 ↓	30.0 ↓	1.4 ↓
	2/0/8	29.8	–	–

[a] Average values calculated form the data obtained during 5 h tests carried out at 550 °C; the arrows next to the given values indicate increase or decrease with the respect to the value obtained with feed gas composition of $CH_4/CO_2/Ar$ = 1/1/8

The results of the tests carried out for HTNi100-Ce catalyst (Fig. 8) showed that the excess of CH_4 in the feed gas had a positive effect on CO_2 conversion, the negative effect on CH_4 conversion and led to higher formation of H_2 when compared to the tests with equimolar feed gas composition, which is in agreement with calculations of thermodynamic equilibrium reported in literature [48, 52–55]. On the other hand, the tests carried out in the excess of CO_2 in the feed caused a decrease in both CH_4 and CO_2 conversions. The distribution of the obtained products was also strongly affected by the feed gas composition and decreased with TOS for DRM runs carried out in the excess of CO_2 and increased with TOS for tests performed in the excess of CH_4.

Similar tests carried out for HTNi100 sample (Table 6) revealed that the excess of CO_2 in the feed gas led to the promotion of CH_4 decomposition and thus increased CH_4 conversions. The Ce addition clearly inhibited CH_4 decomposition and thus increased the selectivity of the process towards DRM, which is reflected in the registered values of H_2/CO close to unity for the tests carried out in the excess of CO_2.

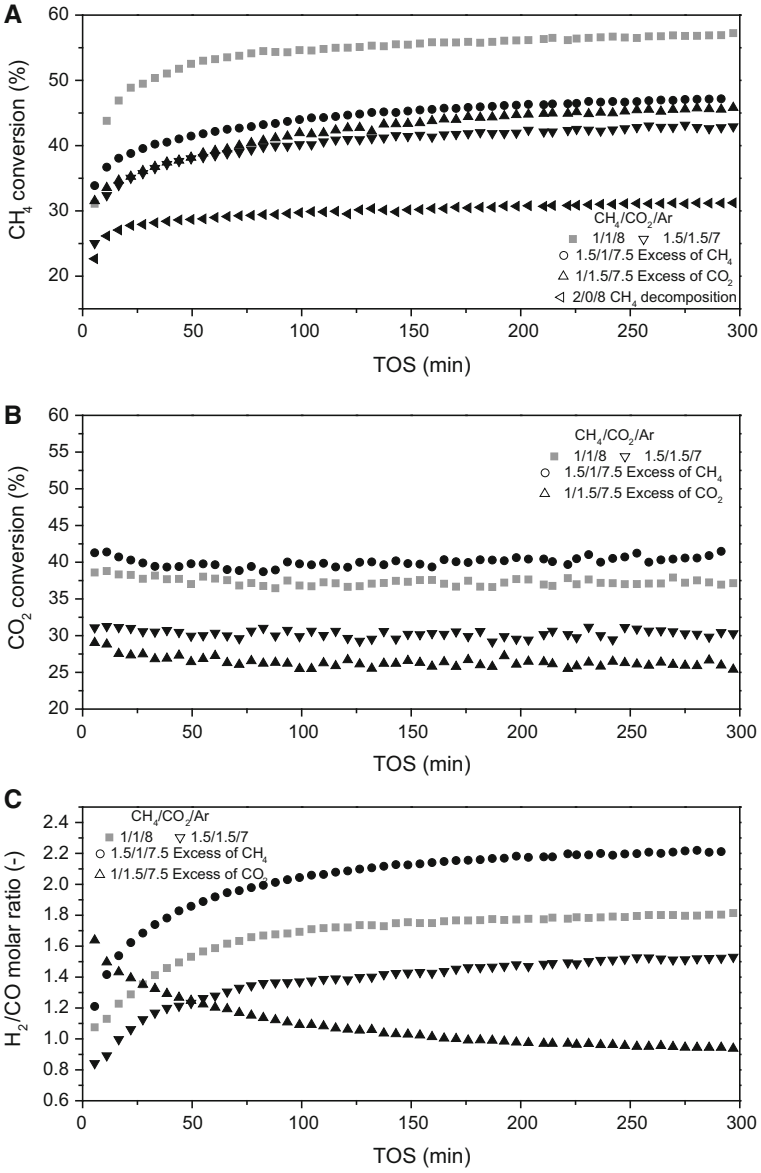

Fig. 8 Catalytic tests over HTNi100-Ce catalyst in DRM reaction at 550 °C for different compositions of feed gas: **a** CH_4 conversion, **b** CO_2 conversion, **c** H_2/CO molar ratio; total flow 100 cm^3/min, GHSV = 20,000 h^{-1}

The results of the tests performed for HTNi25-Ce catalyst are depicted in Fig. 9. Similarly, as for HTNi100-Ce, the excess of CH_4 in the feed had a negative effect on the CH_4 conversion. It, however, barely affected CO_2 conversions, which were at a similar level after around 100 min TOS as for the tests carried out with the

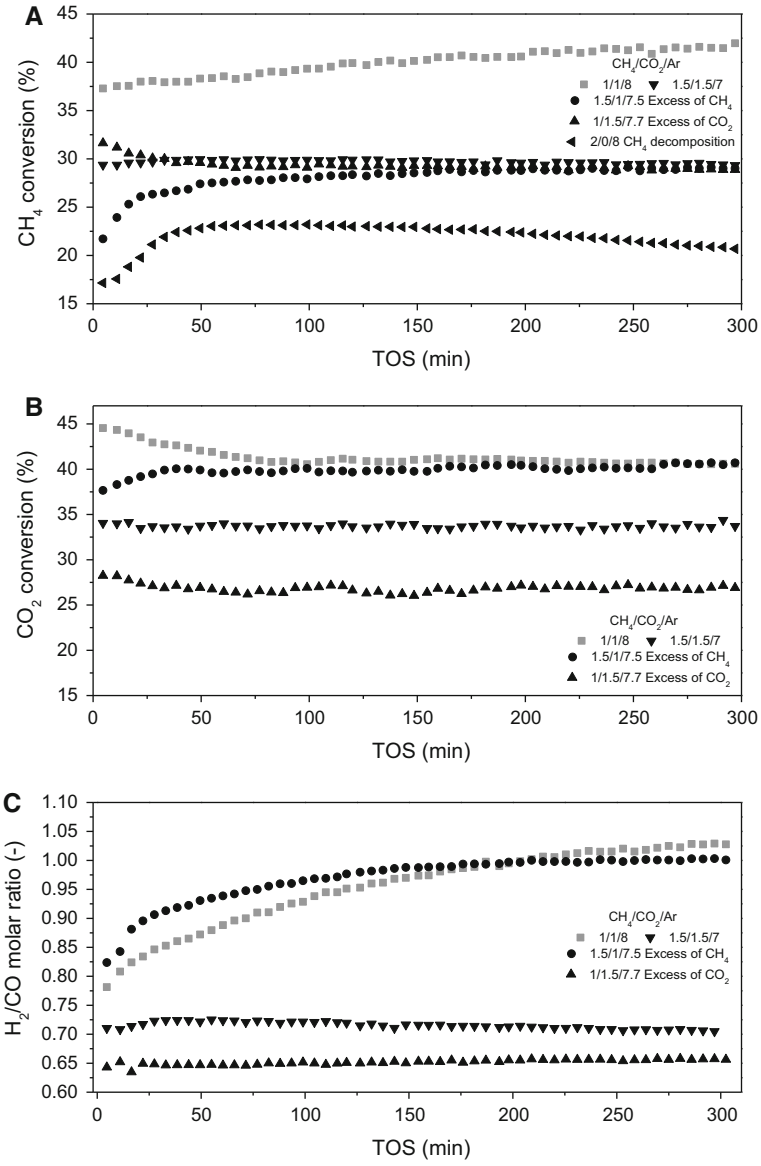

Fig. 9 Catalytic tests over HTNi25-Ce catalyst in DRM reaction at 550 °C for different compositions of feed gas: **a** CH_4 conversion, **b** CO_2 conversion, **c** H_2/CO molar ratio; total flow 100 cm^3/min, GHSV = 20,000 h^{-1}

equimolar feed gas composition of $CH_4/CO_2/Ar = 1/1/8$. The presence of the excess of CO_2 also caused a decrease of both CO_2 and CH_4 conversions and lowered the values of H_2/CO. It is important to mention that the HTNi25-Ce catalyst showed the most stable performance when the excess of CO_2 was introduced to the reactor. According to thermodynamic model calculations [48, 52–55], the application of the

excess of CO_2 should have a positive effect on catalyst stability, as lower formation of carbon deposits should be expected. Additionally, Ce promotion may help to oxidize deposited coke via reverse Boudouard reaction. These two facts may explain the most stable performance of HTNi25-Ce catalyst in the tests carried out with the feed gas composition of $CH_4/CO_2/Ar = 1/1.5/7.5$.

The change in the feed gas composition of $CH_4/CO_2/Ar$ from 1/1/8 to 1.5/1.5/7 led to a decrease in CH_4 and CO_2 conversions, as well as a decrease in H_2/CO ratios for all samples. For the sample HTNi100-Ce, the CH_4 and CO_2 conversions and the product distribution followed the same trends as in the tests carried out with $CH_4/CO_2/Ar$ ratios of 1/1/8. Thus, the increase of methane and CO_2 concentration in the feed gas had a negative effect on the performance of HTNi100-Ce catalyst. On the other hand, the test performed for HTNi25-Ce sample showed that the increase in the concentrations of CO_2 and CH_4 in the feed resulted in a more stable performance of the catalyst, as no changes in CH_4 and CO_2 conversions and H_2/CO ratios were observed during 5 h TOS.

It is important to mention that in case of all catalysts the larger drop in CH_4 conversions than CO_2 conversions was observed when the excess of methane was used. This is also true for the Ce-promoted catalysts tested with decreased dilution of the reagents. For example the change in the feed gas composition from $CH_4/CO_2/Ar = 1/1/8$ to $CH_4/CO_2/Ar = 1.5/1.5/7$ resulted in the drop in CH_4 and CO_2 conversions of ca. 14 and 10% for HTNi100-Ce. The opposite effect was observed for all catalysts tested in the excess of CO_2. This indicates that the CH_4 concentration in the feed influences the occurrence of side reactions, mainly direct methane decomposition, which affects the distribution of the obtained products and accounts for the coke formation. Moreover, a change in the trend observed for HTNi100Ce-catalysts further proves that catalytic activity of hydrotalcite-derived materials is strongly affected by the presence of magnesia and Ce promotion.

Conclusions

The Ni/Mg/Al and Ni/Al hydrotalcite-derived materials were synthesized and subsequently promoted with cerium and applied as catalysts for syngas production in dry reforming of methane at 550, 650 and 750 °C. The characterization of the materials showed that Ce species were present as a separate phase on the materials surface. The proposed method of introduction of Ce species via adsorption from the aqueous solution of $[Ce(EDTA)]^-$ complexes resulted in samples with various Ce loadings. The amount of incorporated Ce species was dependent on Ni loading and increased with the decreasing content of Ni. The reducibility of Ni species was affected by the content of both Ce and Ni, and additionally by the presence of magnesia. For all Ce-promoted catalysts the total basicity decreased in comparison to the unpromoted ones. However, the Ce promotion leads to an increase of the concentration of intermediate and strong basic sites, thus modifying catalytic activity towards the CO_2 adsorption.

The catalytic performance of Ni/Mg/Al hydrotalcite derived materials promoted with cerium is dependent mainly on Ni content and Mg presence but cerium

additionally modifies the activity, selectivity and stability of such catalysts in DRM. The activity of the prepared catalysts towards CH_4 at 550 °C in DRM, as expected, increased with Ni loading. On the other hand, the Ni loading did not influence significantly the CO_2 conversion. The presence of Ce promoter was found to strongly determine both the activity and selectivity of the prepared catalysts. The role of Ce promoter was influenced by the presence of magnesia in the catalytic system. When Mg was absent in the catalyst (the Ni/Al hydrotalcite-derived sample), Ce promotion resulted in an increase of the activity toward CH_4 and a decrease of the CO_2 conversion. For Ni/Mg/Al derived catalysts the effect of Ce promotion varied depending on both the content of nickel and magnesium. The latter had a significant influence on material basicity for both unpromoted and Ce-promoted catalysts. Magnesium also influences the activity of the prepared catalysts towards CO_2, influencing the carbon formation reactions, which was confirmed by the characterization of the spent catalysts. Finally, the addition of Ce increased the total amount of deposited carbon with the simultaneous change in the type and amount of formed carbonaceous deposits from graphitic carbon, inactive in DRM, to amorphous carbon which may contribute to the production of carbon monoxide. Thus, the effect of Ce addition was found to be beneficial for materials stability in DRM.

Finally, two selected catalysts, chosen as representatives of Ni/Al and Ni/Mg/Al hydrotalcite-derived materials, were evaluated for other gas feed composition at 550 °C. For Ce-promoted Ni/Al and Ni/Mg/Al hydrotalcite-derived catalyst the excess of CO_2 in the feed leads to a decrease of both CH_4 and CO_2 conversions. It is important to stress that at the same time, the catalyst stability is enhanced under these conditions. On the other hand, the excess of CH_4 in the feed promoted direct CH_4 decomposition increasing the CH_4 conversion, the H_2 production, but simultaneously also leading to the formation of higher amounts of carbonaceous deposits. The increase of both CH_4 and CO_2 concentration in the feed, led to a decrease in CH_4 and CO_2 conversions and to a higher catalyst stability.

Acknowledgements The work was financed by AGH Grant 11.11.210.213. R. Dębek would like to acknowledge for the financial support the French Embassy in Poland and InnoEnergy PhD School.

References

1. Dubiński J, Wachowicz J, Koteras A (2010) Underground storage of carbon dioxide—the possibilites for using CCS technologies in Polish conditions. Górnictwo i Geologia 5(1):5–19
2. Le Quéré C, Moriarty R, Andrew RM, Canadell JG, Sitch S, Korsbakken JI, Friedlingstein P, Peters GP, Andres RJ, Boden TA, Houghton RA, House JI, Keeling RF, Tans P, Arneth A, Bakker DCE, Barbero L, Bopp L, Chang J, Chevallier F, Chini LP, Ciais P, Fader M, Feely RA, Gkritzalis T, Harris

I, Hauck J, Ilyina T, Jain AK, Kato E, Kitidis V, Klein Goldewijk K, Koven C, Landschützer P, Lauvset SK, Lefèvre N, Lenton A, Lima ID, Metzl N, Millero F, Munro DR, Murata A, Nabel JEMS, Nakaoka S, Nojiri Y, O'Brien K, Olsen A, Ono T, Pérez FF, Pfeil B, Pierrot D, Poulter B, Rehder G, Rödenbeck C, Saito S, Schuster U, Schwinger J, Séférian R, Steinhoff T, Stocker BD, Sutton AJ, Takahashi T, Tilbrook B, van der Laan-Luijkx IT, van der Werf GR, van Heuven S, Vandemark D, Viovy N, Wiltshire A, Zaehle S, Zeng N (2015) Global carbon budget 2015. Earth Syst Sci Data 7(2):349–396. doi:10.5194/essd-7-349-2015

3. International Energy Agency (IEA) (2015) Key trends in CO_2 emissions. Excerpt from: CO_2 emissions from fuel combustion. IEA, Paris
4. Ampelli C, Perathoner S, Centi G (2015) CO_2 utilization: an enabling element to move to a resource- and energy-efficient chemical and fuel production. Philos Trans R Soc Lond A. doi:10.1098/rsta.2014.0177
5. Aresta M, Dibenedetto A (2007) Utilisation of CO_2 as a chemical feedstock: opportunities and challenges. Dalton Trans 28:2975–2992. doi:10.1039/B700658F
6. Hunt AJ, Sin EHK, Marriott R, Clark JH (2010) Generation, capture, and utilization of industrial carbon dioxide. Chemsuschem 3(3):306–322. doi:10.1002/cssc.200900169
7. Wierzbicki D, Debek R, Motak M, Grzybek T, Gálvez ME, Da Costa P (2016) Novel Ni-La-hydrotalcite derived catalysts for CO_2 methanation. Catal Commun 83:5–8. doi:10.1016/j.catcom.2016.04.021
8. Edwards JH, Maitra AM (1995) The chemistry of methane reforming with carbon dioxide and its current and potential applications. Fuel Process Technol 42(2–3):269–289. doi:10.1016/0378-3820(94)00105-3
9. Homs N, Toyir J, de la Piscina PR (2013) Chapter 1—Catalytic processes for activation of CO_2 A2—Suib. In: Steven L (ed) New and future developments in catalysis. Elsevier, Amsterdam, pp 1–26. doi:10.1016/B978-0-444-53882-6.00001-2
10. Lavoie J-M (2014) Review on dry reforming of methane, a potentially more environmentally-friendly approach to the increasing natural gas exploitation. Front Chem. doi:10.3389/fchem.2014.00081
11. Usman M, Wan Daud WMA, Abbas HF (2015) Dry reforming of methane: influence of process parameters—a review. Renew Sustain Energy Rev 45:710–744. doi:10.1016/j.rser.2015.02.026
12. Zhu Y, Zhang S, Chen B, Zhang Z, Shi C (2016) Effect of Mg/Al ratio of NiMgAl mixed oxide catalyst derived from hydrotalcite for carbon dioxide reforming of methane. Catal Today 264:163–170. doi:10.1016/j.cattod.2015.07.037
13. Li N, Shen C, Tan P, Zou Z, Huang W (2015) Effect of phase transformation on the stability of Ni-Mg-Al catlyst for dry reforming of methane. Indian J Chem 54A(10):1198–1205
14. Lin X, Li R, Lu M, Chen C, Li D, Zhan Y, Jiang L (2015) Carbon dioxide reforming of methane over Ni catalysts prepared from Ni-Mg-Al layered double hydroxides: influence of Ni loadings. Fuel 162:271–280. doi:10.1016/j.fuel.2015.09.021
15. Tan P, Gao Z, Shen C, Du Y, Li X, Huang W (2014) Ni-Mg-Al solid basic layered double oxide catalysts prepared using surfactant-assisted coprecipitation method for CO_2 reforming of CH_4. Chin J Catal 35(12):1955–1971. doi:10.1016/S1872-2067(14)60171-6
16. Touahra F, Sehailia M, Ketir W, Bachari K, Chebout R, Trari M, Cherifi O, Halliche D (2015) Effect of the Ni/Al ratio of hydrotalcite-type catalysts on their performance in the methane dry reforming process. Appl Petrochem Res. doi:10.1007/s13203-015-0109-y
17. Min J-E, Lee Y-J, Park H-G, Zhang C, Jun K-W (2015) Carbon dioxide reforming of methane on Ni–MgO–Al_2O_3 catalysts prepared by sol–gel method: effects of Mg/Al ratios. J Ind Eng Chem 26:375–383. doi:10.1016/j.jiec.2014.12.012
18. Gonzalez AR, Asencios YJO, Assaf EM, Assaf JM (2013) Dry reforming of methane on Ni-Mg-Al nano-spheroid oxide catalysts prepared by the sol-gel method from hydrotalcite-like precursors. Appl Surf Sci 280:876–887. doi:10.1016/j.apsusc.2013.05.082
19. Daza CE, Cabrera CR, Moreno S, Molina R (2010) Syngas production from CO_2 reforming of methane using Ce-doped Ni-catalysts obtained from hydrotalcites by reconstruction method. Appl Catal A 378(2):125–133. doi:10.1016/j.apcata.2010.01.037
20. Daza CE, Gallego J, Mondragón F, Moreno S, Molina R (2010) High stability of Ce-promoted Ni/Mg-Al catalysts derived from hydrotalcites in dry reforming of methane. Fuel 89(3):592–603. doi:10.1016/j.fuel.2009.10.010
21. Daza CE, Gallego J, Moreno JA, Mondragón F, Moreno S, Molina R (2008) CO_2 reforming of methane over Ni/Mg/Al/Ce mixed oxides. Catal Today 133–135:357–366. doi:10.1016/j.cattod.2007.12.081

22. Daza CE, Moreno S, Molina R (2010) Ce-incorporation in mixed oxides obtained by the self-combustion method for the preparation of high performance catalysts for the CO_2 reforming of methane. Catal Commun 12(3):173–179. doi:10.1016/j.catcom.2010.09.012
23. Daza CE, Moreno S, Molina R (2011) Co-precipitated Ni–Mg–Al catalysts containing Ce for CO_2 reforming of methane. Int J Hydrogen Energy 36(6):3886–3894. doi:10.1016/j.ijhydene.2010.12.082
24. Liu H, Wierzbicki D, Debek R, Motak M, Grzybek T, Da Costa P, Gálvez ME (2016) La-promoted Ni-hydrotalcite-derived catalysts for dry reforming of methane at low temperatures. Fuel 182:8–16. doi:10.1016/j.fuel.2016.05.073
25. Serrano-Lotina A, Rodríguez L, Muñoz G, Martin AJ, Folgado MA, Daza L (2011) Biogas reforming over La-NiMgAl catalysts derived from hydrotalcite-like structure: influence of calcination temperature. Catal Commun 12(11):961–967. doi:10.1016/j.catcom.2011.02.014
26. Yu X, Wang N, Chu W, Liu M (2012) Carbon dioxide reforming of methane for syngas production over La-promoted NiMgAl catalysts derived from hydrotalcites. Chem Eng J 209:623–632. doi:10.1016/j.cej.2012.08.037
27. Tsyganok AI, Inaba M, Tsunoda T, Uchida K, Suzuki K, Takehira K, Hayakawa T (2005) Rational design of Mg–Al mixed oxide-supported bimetallic catalysts for dry reforming of methane. Appl Catal A 292:328–343. doi:10.1016/j.apcata.2005.06.007
28. Zhang J, Wang H, Dalai AK (2008) Effects of metal content on activity and stability of Ni-Co bimetallic catalysts for CO_2 reforming of CH_4. Appl Catal A 339(2):121–129. doi:10.1016/j.apcata.2008.01.027
29. Long H, Xu Y, Zhang X, Hu S, Shang S, Yin Y, Dai X (2013) Ni-Co/Mg-Al catalyst derived from hydrotalcite-like compound prepared by plasma for dry reforming of methane. J Energy Chem 22(5):733–739. doi:10.1016/S2095-4956(13)60097-2
30. Lucrédio AF, Assaf JM, Assaf EM (2014) Reforming of a model sulfur-free biogas on Ni catalysts supported on Mg(Al)O derived from hydrotalcite precursors: effect of La and Rh addition. Biomass Bioenergy 60:8–17. doi:10.1016/j.biombioe.2013.11.006
31. Dębek R, Galvez ME, Launay F, Motak M, Grzybek T, Da Costa P (2016) Low temperature dry methane reforming over Ce, Zr and CeZr promoted Ni–Mg–Al hydrotalcite-derived catalysts. Int J Hydrogen Energy 41(27):11616–11623. doi:10.1016/j.ijhydene.2016.02.074
32. Dębek R, Motak M, Duraczyska D, Launay F, Galvez ME, Grzybek T, Da Costa P (2016) Methane dry reforming over hydrotalcite-derived Ni-Mg-Al mixed oxides: the influence of Ni content on catalytic activity, selectivity and stability. Catal Sci Technol 6(17):6705–6715. doi:10.1039/C6CY00906A
33. Dębek R, Zubek K, Motak M, Da Costa P, Grzybek T (2015) Effect of nickel incorporation into hydrotalcite-based catalyst systems for dry reforming of methane. Res Chem Intermed 41(12):9485–9495. doi:10.1007/s11164-015-1973-x
34. Cavani F, Trifirò F, Vaccari A (1991) Hydrotalcite-type anionic clays: preparation, properties and applications. Catal Today 11(2):173–301. doi:10.1016/0920-5861(91)80068-K
35. Tichit D, Coq B (2003) Catalysis by hydrotalcites and related materials. CATTECH 7(6):206–217. doi:10.1023/b:catt.0000007166.65577.34
36. Goh K-H, Lim T-T, Dong Z (2008) Application of layered double hydroxides for removal of oxyanions: a review. Water Res 42(6–7):1343–1368. doi:10.1016/j.watres.2007.10.043
37. Rives V (2002) Characterisation of layered double hydroxides and their decomposition products. Mater Chem Phys 75(1–3):19–25. doi:10.1016/S0254-0584(02)00024-X
38. Rives V, Carriazo D, Martín C (2010) Heterogeneous catalysis by polyoxometalate-intercalated layered double hydroxides. In: Gil A, Korili AS, Trujillano R, Vicente AM (eds) Pillared clays and related catalysts. Springer, New York, pp 319–397. doi:10.1007/978-1-4419-6670-4_12
39. Forano C, Costantino U, Prévot V, Gueho CT (2013) Chapter 14.1—Layered double hydroxides (LDH). In: Faïza B, Gerhard L (eds) Developments in clay science, vol 5. Elsevier, Amsterdam, pp 745–782. doi:10.1016/B978-0-08-098258-8.00025-0
40. Debecker DP, Gaigneaux EM, Busca G (2009) Exploring, tuning, and exploiting the basicity of hydrotalcites for applications in heterogeneous catalysis. Chem Eur J 15(16):3920–3935. doi:10.1002/chem.200900060
41. Dębek R, Radlik M, Motak M, Galvez ME, Turek W, Da Costa P, Grzybek T (2015) Ni-containing Ce-promoted hydrotalcite derived materials as catalysts for methane reforming with carbon dioxide at low temperature—on the effect of basicity. Catal Today 257:59–65. doi:10.1016/j.cattod.2015.03.017

42. Di Cosimo JI, Díez VK, Xu M, Iglesia E, Apesteguía CR (1998) Structure and surface and catalytic properties of Mg-Al basic oxides. J Catal 178(2):499–510. doi:10.1006/jcat.1998.2161
43. Gac W (2011) Acid–base properties of Ni–MgO–Al_2O_3 materials. Appl Surf Sci 257(7):2875–2880. doi:10.1016/j.apsusc.2010.10.084
44. Koo KY, S-h Lee, Jung UH, Roh H-S, Yoon WL (2014) Syngas production via combined steam and carbon dioxide reforming of methane over Ni–Ce/$MgAl_2O_4$ catalysts with enhanced coke resistance. Fuel Process Technol 119:151–157. doi:10.1016/j.fuproc.2013.11.005
45. H-P Wu, W-J Li, Guo L, Pan Y-F, Xu X-F (2011) Effect of promoter species and precursors on catalytic activity of alkali metal promoted NiAl mixed oxides for N_2O decomposition. J Fuel Chem Technol 39(7):550–555. doi:10.1016/S1872-5813(11)60034-0
46. H-p Wu, Qian Z-y Xu, X-f X-l, Xu (2011) N_2O decomposition over K-promoted NiAl mixed oxides derived from hydrotalcite-like compounds. J Fuel Chem Technol 39(2):115–121. doi:10.1016/S1872-5813(11)60013-3
47. Djebarri B, Gonzalez-Delacruz VM, Halliche D, Bachari K, Saadi A, Caballero A, Holgado JP, Cherifi O (2013) Promoting effect of Ce and Mg cations in Ni/Al catalysts prepared from hydrotalcites for the dry reforming of methane. Reac Kinet Mech Cat 111(1):259–275. doi:10.1007/s11144-013-0646-2
48. Nikoo MK, Amin NAS (2011) Thermodynamic analysis of carbon dioxide reforming of methane in view of solid carbon formation. Fuel Process Technol 92(3):678–691. doi:10.1016/j.fuproc.2010.11.027
49. Tsyganok AI, Tsunoda T, Hamakawa S, Suzuki K, Takehira K, Hayakawa T (2003) Dry reforming of methane over catalysts derived from nickel-containing Mg-Al layered double hydroxides. J Catal 213(2):191–203
50. Zhang ZL, Verykios XE (1994) Carbon dioxide reforming of methane to synthesis gas over supported Ni catalysts. Catal Today 21(2):589–595. doi:10.1016/0920-5861(94)80183-5
51. Hu YH, Ruckenstein E (2004) Catalytic conversion of methane to synthesis gas by partial oxidation and CO_2 reforming. In: Hohn KL, Schmidt LD (eds) Advances in catalysis, vol 48. Academic Press, New York, pp 297–345. doi:10.1016/S0360-0564(04)48004-3
52. Sun Y, Ritchie T, Hla SS, McEvoy S, Stein W, Edwards JH (2011) Thermodynamic analysis of mixed and dry reforming of methane for solar thermal applications. J Nat Gas Chem 20(6):568–576. doi:10.1016/S1003-9953(10)60235-6
53. Chein RY, Chen YC, Yu CT, Chung JN (2015) Thermodynamic analysis of dry reforming of CH4 with CO2 at high pressures. J Nat Gas Sci Eng 26:617–629. doi:10.1016/j.jngse.2015.07.001
54. Istadi A, Amin NAS (2005) Co-generation of C_2 hydrocarbons and synthesis gases from methane and carbon dioxide: a thermodynamic analysis. J Nat Gas Chem 14:140–150
55. Özkara-Aydınoğlu Ş (2010) Thermodynamic equilibrium analysis of combined carbon dioxide reforming with steam reforming of methane to synthesis gas. Int J Hydrogen Energy 35(23):12821–12828. doi:10.1016/j.ijhydene.2010.08.134